RSC Advances

PAPER

View Article Online
View Journal | View Issue

Cite this: *RSC Adv.*, 2018, **8**, 39929

Pb^{II}-catalyzed transformation of aromatic nitriles to heptanitrogen anions *via* sodium azide: a combined experimental and theoretical study†

Rong-Yi Huang,*[a] Chao Zhang,[a] Da Yan,[a] Zhi Xiong,[a] Heng Xu*[a] and Xiao-Ming Ren*[b]

Under hydrothermal conditions, an open-chain N_7^{3-} anion stabilized in a metal–organic framework (MOF) was achieved for the first time *via* the *in situ* reaction of 4-fluorobenzonitrile and sodium azide with Pb^{2+} ion as catalyst. The anion with C_{2h} symmetry in the MOF was studied by FT-IR, single-crystal XRD and theoretical calculations. Thermal analysis results demonstrated the stability of the anion in the MOF below 430 °C and a high energy content of 8.61 kJ g^{-1}. The anion is also a good reducing agent. It can easily react with basic $KMnO_4$ solution. Moreover, the present study indicates that the Pb^{2+} ion activates the azide rather than nitrile in the *in situ* reaction of nitriles with azides to form polynitrogen and this mechanism is a distinct contradiction with the previous results in which the nitrile reacts with azide in the presence of transition metal ions. Our findings may open a new avenue towards the synthesis and capture of polynitrogen compounds.

Received 13th October 2018
Accepted 26th November 2018

DOI: 10.1039/c8ra08486f

rsc.li/rsc-advances

Introduction

Metal–organic frameworks (MOFs) have attracted enormous attention for not only fundamental interest but also applied research, such as gas separation, gas storage, catalysis, chemical sensing and drug delivery,[1–10] and this is due to the unique nature of the porosity.[11] Several surprising studies have recently underscored the potential important application of nitrogen-rich MOFs in the area of energetic materials.[12–15] In particular, the metal ions, *via* coordinating with nitrogen-rich ligands, can be easily constructed as energetic MOFs and most of them possess lower sensitivities.[16] To date, albeit that many MOFs based on energetic ligands, including hydrazines, triazoles and tetrazoles, have been designed and synthesized as interesting candidates for primary or secondary explosives,[15–24] no significant progress in MOFs involving polynitrogen ligands (N_n, with n more than three) has been achieved due to the assembly difficulties and intrinsic instability of polynitrogen species. In this context, it is a significant challenge to obtain more stable polynitrogen ligands and reveal the reaction mechanism to chemists, since nitrogen atoms do not tend to generate stable multi-atom rings or long chains and most of the reaction intermediates are too active to be captured. Single-crystal XRD is a powerful tool for exploring a reaction mechanism and directly provides information on the nature of reaction intermediates.[25–27] However, the precondition is based on the fact that the active intermediates must be captured in their crystalline state. Recently, using single-crystal XRD analysis, Lu and co-workers have demonstrated that metal ion catalysis plays a critical role in the *in situ* reaction of tetrazole formation[28] and it has been found that the common [2 + 3] cycloaddition reaction of nitrile with azide to form tetrazole was easily achieved in water using metal ions as a Lewis acid catalyst[29–32] and density-functional theory (DFT) calculations disclosed that the activation of nitrile using Zn^{2+} ions is the critical step for *in situ* tetrazole formation,[33] such a mechanism was further supported *via* the capture of a crystalline reaction intermediate during the experiment.[28]

Currently, a large number of studies have been focused on the *in situ* formation of metal–tetrazole complexes using transition metal ions, *e.g.* Zn^{2+}, Co^{2+}, Cd^{2+} and Mn^{2+}, as the Lewis acid catalyst.[29–32] In this study, we noted that the halides or pseudohalides of transition metal ions and the main group Pb^{2+} ion show different solubility in water. This fact indicates that there exists a distinct coordination interaction between the metal ion and halide or pseudohalide anions between the transition metal ions and main group Pb^{2+} ion. Consequently, it is possible to obtain different products if the transition metal ions are replaced by the main group Pb^{2+} ion during the *in situ* reaction of nitrile with azide to form tetrazole. We attempted to explore the reaction of nitrile and azide in the presence of the

[a]*Anhui Key Laboratory of Functional Coordination Compounds, School of Chemistry and Chemical Engineering, Anqing Normal University, Anqing 246011, P. R. China. E-mail: huangry@aqnu.edu.cn*

[b]*State Key Laboratory of Materials-Oriented Chemical Engineering, College of Chemistry & Molecular Engineering, Nanjing Tech University, Nanjing, 210009, P. R. China. E-mail: xmren@njtech.edu.cn*

† Electronic supplementary information (ESI) available: CCDC 1487965–1487967. For ESI and crystallographic data in CIF or other electronic format see DOI: 10.1039/c8ra08486f

main group Pb^{2+} ion. Surprisingly, a new open-chain poly-nitrogen anion was isolated in the water instead of the *in situ* formation of tetrazole. We further designed a reaction system, by which we successfully captured three interrelated intermediate products, $H_3O[Pb_8(\mu_6\text{-}N_7)(\mu_4\text{-}O)_2(\mu_6\text{-}ox)(\mu_7\text{-}CHDA)_4]\cdot 4H_2O$ (**MOF-N$_7$**), $Pb_3(N_3)_6$ (**α-Pb(N$_3$)$_2$**) and $[Pb_2(\mu_4\text{-}O)(FBA)_2]\cdot 2H_2O$ (**Pb-FBA**) (HFBA = 4-fluorobenzoic acid; H_2CHDA = 1,3-cyclohexane-dicarboxylic acid; H_2ox = oxalate acid), the crystal structures of which were characterized. Our results reveal that the azide ion, rather than the nitrile was activated by the Pb^{2+} ion and this was distinct from that previously reported reaction catalyzed by transition metal ions.[28,33]

Experimental and computational sections

Caution

Azides and **MOF-N$_7$** are a highly energetic. They should be handled only on a very small scale and must be handled with special caution.

Materials and general methods

All chemicals used were obtained commercially and used without further purification. C, H and N microanalyses were performed on a Vario EL III elementary analyzer. FT-IR spectra (KBr pellet) were recorded in the range 400–4000 cm^{-1} on an iS50 FT-IR (Nicolet) spectrometer. Powder X-ray diffraction pattern (PXRD) was performed on a Rigaku D/max-RA rotating anode X-ray diffractometer at room temperature. N_2 sorption isotherm was obtained on the Belsorp MAX volumetric adsorption equipment. Thermogravimetric analysis and differential scanning calorimetry (TGA/DSC) were determined on a Netzsch STA-409PC analyzer in flowing N_2 with a linear heating rate of 10 °C min^{-1}.

Synthesis of MOF-N$_7$, α-Pb(N$_3$)$_2$ and Pb-FBA

$H_3O[Pb_8(\mu_6\text{-}N_7)(\mu_4\text{-}O)_2(\mu_6\text{-}ox)(\mu_7\text{-}CHDA)_4]\cdot 4H_2O$ (MOF-N$_7$). A mixture of $Pb(NO_3)_2$, (0.0662 g, 0.2 mmol), H_2CHDA (0.0172 g, 0.1 mmol), 4-FBN (0.0121 g, 0.1 mmol), NaN_3 (0.0130 g, 0.2 mmol), NaOH (0.0080 g, 0.2 mmol) and H_2O (14 mL) was sealed in a 25 mL Teflon-lined stainless steel container. The reactor was heated to 160 °C for 96 h, and then slowly cooled down to room temperature. Colorless block crystals of **MOF-N$_7$** were isolated *via* filtration and rinsed with distilled water several times in 35% yield (based on $Pb(NO_3)_2$). $C_{34}H_{51}N_7O_{27}Pb_8$ (2647.41): calc. C, 15.43; H, 1.94 N, 3.70; found C, 15.38; H, 1.99; N, 3.65%. FT-IR (KBr pellet, cm^{-1}): 3446(w), 2915(m), 2849(m), 2061(m), 1585(s), 1544(s), 1506(s), 1399(s), 1354(m), 1341(m), 1320(m), 1294(m), 1268(m), 1250(m), 1226(m), 1185(m), 1140(m), 1027(m), 959(m), 916(m), 766(m), 714(m), 685(m), 655(m), 566(m), 520(m), 487(m).

$Pb_3(N_3)_6$ (α-Pb(N$_3$)$_2$). The preparation of **α-Pb(N$_3$)$_2$** was carried out using the procedure for preparing **MOF-N$_7$** with the addition of 4-FBN not included. Yellow rod crystals of **α-Pb(N$_3$)$_2$** were isolated *via* filtration and rinsed with distilled water several times in 70% yield (based on NaN_3). $N_{18}Pb_3$ (873.75): calc. N, 28.86; found N, 28.78%. FT-IR (KBr pellet, cm^{-1}): 2036(s), 1384(m), 1328(w), 1128(w), 1043(w), 669(w), 632(w), 606(w), 434(w).

$[Pb_2(\mu_4\text{-}O)(FBA)_2]\cdot 2H_2O$ (Pb-FBA). **Pb-FBA** was obtained *via* the reaction of $Pb(NO_3)_2$ with 4-FBN and NaN_3 under the same reaction conditions used for the preparation of **MOF-N$_7$**. Colorless rod crystals of **Pb-FBA** were isolated *via* filtration and rinsed with distilled water several times in 65% yield (based on 4-FBN). $C_{14}H_{12}F_2O_7Pb_2$ (744.64): calc. C, 22.58; H, 1.62; found C, 22.52; H, 1.75%. FT-IR (KBr pellet, cm^{-1}): 3448(m), 3086(w), 2926(m), 1606(s), 1552(s), 1525(s), 1509(m), 1492(m), 1298(w), 1239(m), 1227(m), 1215(m), 1151(m), 1088(w), 1013(w), 857(m), 782(s), 688(w), 669(w), 610(s), 547(w), 528(w), 492(w), 431(m).

X-ray crystallography study

Single crystal X-ray diffraction analyses of **MOF-N$_7$**, **α-Pb(N$_3$)$_2$** and **Pb-FBA** were performed on a Bruker SMART APEX II CCD diffractometer with graphite monochromated Mo-Kα radiation (λ = 0.71073 Å) at room temperature. The empirical absorption corrections based on psi-scan were carried out. The crystal diffraction data were integrated with the Bruker SAINT program. Sadabs program was used for absorption correction. The crystal structures were solved *via* direct methods and all non-hydrogen atoms were refined anisotropically using the full-matrix least-squares technique on F^2 using the SHELXL-2014.[34] All hydrogen atoms on the carbon atoms were calculated in their idealized positions and refined using the riding model. The largest diffraction peak and hole are attributed to the ghost peaks of the heavy lead atom. The ISOR restraint was applied to the disordered N1, C5 and C6 atoms in **MOF-N$_7$** (PLAT342_ALERT_3_B checkCIF alert for **MOF-N$_7$** due to the disordered C5 and C6 atoms). At the same time, the SIMU and DELU restraints were also applied to the N1, N2, N3 and N4 atoms in **MOF-N$_7$**. All these restraints can make the ADP values of the disordered atoms in **MOF-N$_7$** more reasonable. Furthermore, the guest water molecules in **MOF-N$_7$** and **Pb-FBA** and hydronium ions in **MOF-N$_7$** in the corresponding frameworks are highly distorted and impossible to refine *via* conventional discrete atom models (PLAT601_ALERT_2_A checkCIF alert for **MOF-N$_7$**, and PLAT601_ALERT_2_B checkCIF alert for **Pb-FBA**). The final formulas for **MOF-N$_7$** and **Pb-FBA** were obtained from the PLATON results in combination with the experimental results obtained from elemental analysis (EA) and thermogravimetric analysis (TGA). The pertinent crystal parameters, data collection and refinement as well as the selected bond lengths and angles with their estimated deviations for **MOF-N$_7$**, **α-Pb(N$_3$)$_2$** and **Pb-FBA** are summarized in the Tables 1 and S1–S3,† respectively.

Computational details

All computations reported in the present work were performed using the Gaussian09 D.01 program package.[35] Density-functional theory (DFT) calculations were carried out using the popular B3LYP method.[36,37] The Stuttgart–Dresden (SDD)[38] effective core potential (ECP) was employed for Pb atoms, while the 6-31+G(d,p) basis set was used for C, H, O and N atoms. To verify the activation of the azide ion by the Pb^{2+} ion, we

Table 1 Crystallographic data and structure refinement summary for MOF-N_7, α-$Pb(N_3)_2$ and Pb-FBA

Complexes	**MOF-N_7**	**α-$Pb(N_3)_2$**	**Pb-FBA**
Formula	$C_{34}H_{51}N_7O_{27}Pb_8$	$N_{18}Pb_3$	$C_{14}H_{12}F_2O_7Pb_2$
Formula weight	2647.41	873.75	744.64
Crystal system	Monoclinic	Orthorhombic	Tetragonal
Space group	*C*2/*m*	*Pnma*	$I4_1/a$
a (Å)	8.1312(6)	6.6300(2)	24.6059(4)
b (Å)	29.931(3)	16.2630(6)	24.6059(4)
c (Å)	11.5601(9)	11.3428(4)	10.7731(2)
β (°)	102.974(5)	90	90
Volume ($Å^3$)	2741.7(4)	1223.02(7)	6522.6(2)
Z	2	4	16
T (K)	293(2)	296(2)	296(2)
D_{calcd} (mg m^{-3})	3.096	4.745	2.886
F(000)	2250	1488	5024
θ range (°)	3.268 to 25.050	2.189 to 25.042	1.655 to 25.049
Reflections collected	6743	3906	34 531
Independent reflections	2468[$R_{int} = 0.0476$]	1111[$R_{int} = 0.0426$]	2888[$R_{int} = 0.0384$]
Data/restraints/parameters	2468/41/170	1111/0/104	2888/0/208
Goodness of fit on F^2	1.003	1.000	1.001
Final *R* indices [$I > 2\sigma(I)$]	$R_1 = 0.0419^a$	$R_1 = 0.0276^a$	$R_1 = 0.0183^a$
	$wR_2 = 0.1255^b$	$wR_2 = 0.0711^b$	$wR_2 = 0.0462^b$
R indices (all data)	$R_1 = 0.0541^a$	$R_1 = 0.0319^a$	$R_1 = 0.0268^a$
	$wR_2 = 0.1310^b$	$wR_2 = 0.0731^b$	$wR_2 = 0.0489^b$
Largest diff. peak and hole (e $Å^{-3}$)	2.526 and −1.818	2.084 and −1.259	0.548 and −0.875
CCDC reference number	1487965	1487966	1487967

^{a} $R_1 = \sum||F_o| - |F_c||/\sum|F_o|$. ^{b} $wR_2 = |\sum w(|F_o|^2 - |F_c|^2)|/\sum|w(F_o)^2|^{1/2}$, $w = 1/[\sigma^2(F_o^2) + (aP)^2 + bP]$. $P = (F_o^2 + 2F_c^2)/3$.

considered two different activated models of Pb^{2+} with N_3^- and 4-FBN. The DFT calculations were performed on the above **Pb⋯N_3** and **Pb⋯4-FBN** associations (Fig. S1†). The additional calculations were also performed on monomeric Pb^{2+}, N_3^- and 4-FBN. For all the species studied here, the geometries were optimized and the final compounds correspond to minima since no imaginary frequencies were found. The SMD[39] solvation model was selected for H_2O effects. The interaction energies of both associations were determined from the energy difference between the association and monomers, considering the zero point vibrational energy, ZPE. The basis-set superposition error, BSSE was computed using the counterpoise method of Boys and Bernardi.[40] Additionally, to further aid in the interpretation of the reaction mechanism of 4-FBN and NaN_3 with Pb^{2+} ion as the Lewis acid catalyst, the molecular electrostatic potential as well as the electrostatic potential basins analysis by means of the Multiwfn program[41] were obtained based on the optimized stable **Pb⋯N_3** and 4-FBN, respectively. Additionally, to clarify the nature of N_7^{3-} anion and **MOF-N_7**, DFT calculations were performed on the N_7^{3-} anion (**N_7^{3-}-C_{2h}**) and a minor calculation model was selected, $[Pb_{16}(O)_4(ox)_4(N_7)(CH_3COO)_{14}(CH_3COOH)_2]^-$ (**MOF-$N_{7'}$**) from the crystal structure of **MOF-N_7** (Fig. S2†). The optimized stable structure of the N_7^{3-} anion was also obtained. The stable N_7^{3-} anion (**N_7^{3-}-C_{2v}**) possessed C_{2v} symmetry. For **MOF-$N_{7'}$**, only the hydrogen positions were optimized. Based on the Multiwfn procedure, the characteristics of the bond critical points (BCPs) of all the N–N and Pb–N bonds in **MOF-$N_{7'}$** were also analysed with the atoms in molecules (AIM) methodology.[42] Furthermore, the dissociation energies obtained for **N_7^{3-}-C_{2h}** and **N_7^{3-}-C_{2v}** were established *via* $\Delta E_{dis} = E(N_7^{3-}) - 7/2E(N_2)$ at the B3LYP/6-31+G(d,p) level of theory.

Results and discussion

Synthesis

It should be noted that the first N_7^{3-} anion stabilized in the **MOF-N_7** was isolated *via* the *in situ* reaction of 4-fluorobenzonitrile (4-FBN) and sodium azide using Pb^{2+} ion as the Lewis acid catalyst under hydrothermal condition. Therefore, a few comparative experiments were considered to show the predominant influence factors to generate the N_7^{3-} anion. The results demonstrate that the *in situ* reaction can be affected by several factors such as the metal ions and the auxiliary organic carboxylate ligands. Under the similar reaction conditions used for the preparation of **MOF-N_7**, when the Pb^{2+} ion in the *in situ* reaction was replaced by other metal ions, *e.g.* Zn^{2+}, Cd^{2+}, Co^{2+}, Ni^{2+}, Cu^{2+}, Ag^+, Mn^{2+} and so on, as the Lewis acid catalyst, the N_7^{3-} anion could not be isolated, so the Pb^{2+} ion plays a key role in the *in situ* generated N_7^{3-} anion. Additionally, the auxiliary H_2CHDA also plays a crucial role in this reaction, as the N_7^{3-} anion was not obtained when the H_2CHDA was substituted by other organic carboxylate ligands or removed from the reaction mixture. However, when the 4-FBN in the reaction was replaced by other nitriles, *e.g.* benzonitrile, 4-cyanopyridine, 4-aminobenzonitrile, 4-methylbenzonitrile, 4-methoxybenzonitrile, 4-(imidazol-1-ylmethyl)benzonitrile, 1-(4-cyanophenyl)imidazole, 4-chlorobenzonitrile and 1,4-benzenedicarbonitrile, the target **MOF-N_7** can also be obtained under the same reaction conditions.

Description of crystal structure

Crystal structure of MOF-N_7. Crystals of **MOF-N_7** were achieved *via* the hydrothermal reaction of $Pb(NO_3)_2$ with H_2CHDA, 4-FBN and NaN_3 in water at 160 °C for 96 h (see the ESI†). The phase purity of **MOF-N_7** was examined using powder X-ray diffraction (Fig. S3†). **MOF-N_7** crystallizes in the monoclinic space group *C*2/*m* and presents a 3D pillared-layer metal–organic framework containing the *in situ* formed N_7^{3-} anion. The asymmetric unit in **MOF-N_7** (Fig. S4a†) was comprised of three independent Pb^{2+} ions (Pb1 and Pb2 located on the crystallographic mirror plane and two-fold axis, respectively), one $CHDA^{2-}$ anion, one half O^{2-} anion located on the two-fold axis and one quarter *in situ* generated ox^{2-} anion and the N_7^{3-} anion all located on the crystallographic mirror plane and two-fold axis. The Pb1 and Pb3 ions are seven-coordinated whereas the Pb2 ion was eight-coordinated. The μ_4-O^{2-} anions link the adjacent Pb^{2+} ions (Pb1 and Pb3) to give a rare cationic cluster $[Pb_6O_2]^{8+}$ located on the crystallographic inverse center. Furthermore, these cationic clusters are linked *via* the μ_6-ox^{2-} ligands to present a definite 1D cationic chain (Fig. S4b†). The adjacent Pb2 ions are also bridged *via* μ_7-$CHDA^{2-}$ carboxylates to form a distinct 1D anionic chain (Fig. S4c†). The adjacent cationic and anionic chains are not isolated but linked together by the carboxylate groups of the $CHDA^{2-}$ ligands into a 2D cationic layer parallel to the *ab* plane (Fig. S4d†). These layers are further linked *via* the linear μ_6-N_7^{3-} anion *via* the Pb1–N1 and Pb3–N1 bonds to generate a 3D pillared-layer open framework (Fig. 1 and S4e†). The disordered H_2O molecules and H_3O^+ ions are trapped in the channels and further reinforce the open framework *via* weak intermolecular interactions. This can be also supported by the N_2 sorption isotherm measured at 77 K (Fig. 2). After removal of the disordered H_2O molecules and H_3O^+ ions, the **MOF-N_7** framework can be only stable up to approximately 0.009 P_0 and then started to abruptly decompose, accompanied by the release of N_2, which was due to the decomposition of the N_7^{3-} anion. The above result presents that the disordered groups in the channels of **MOF-N_7** play a crucial role in the stabilizing N_7^{3-} anion *via* weak intermolecular interactions as well as the coordination interaction between the Pb^{2+} ion and N_7^{3-} anion.

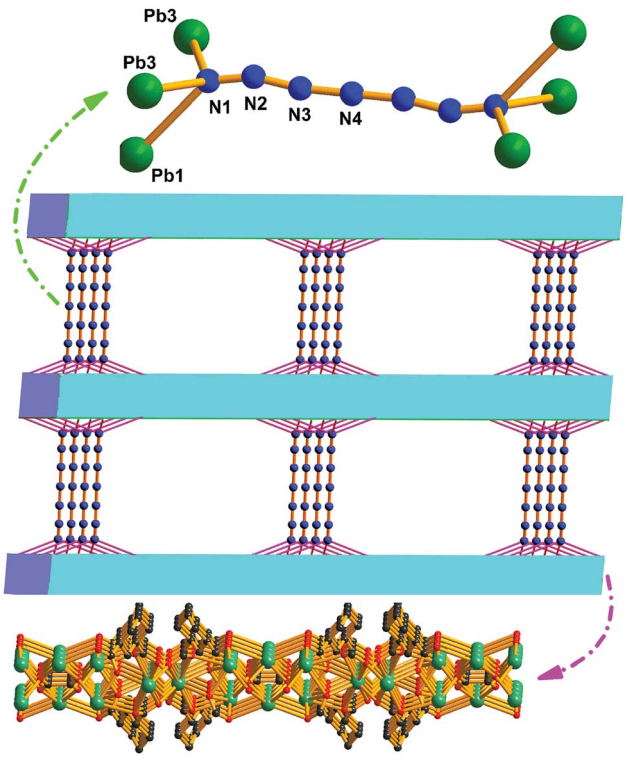

Fig. 1 The 3D open framework constructed from the 2D cationic layers and N_7^{3-} anionic pillars of MOF-N_7.

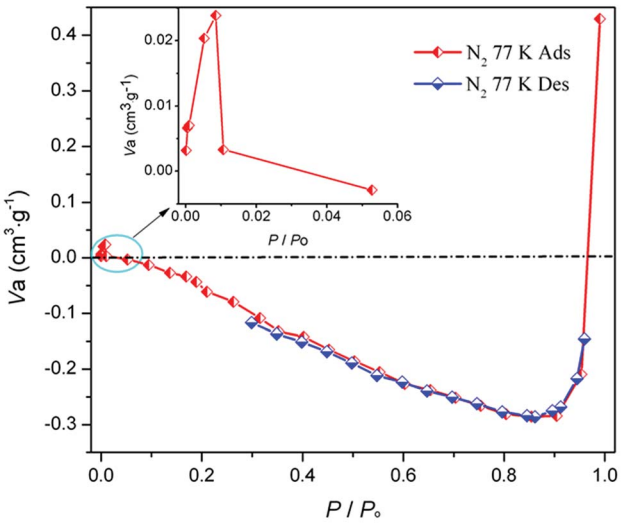

Fig. 2 The N_2 sorption isotherm of MOF-N_7 at 77 K.

Moreover, this is the first N_7^{3-} anion stabilized in a MOF *via* coordination to the Pb^{2+} ions located on the 2D metal–organic cationic layers, which possesses C_{2h} symmetry. The N1–N2, N2–N3 and N3–N4 bond lengths are 1.198(31), 1.261(39) and 1.191(30) Å respectively. The bond angles of ∠N–N–N are at the range of 165.2(3)–180.0(2)° (Table S1†). The N_7^{3-} anion structure can be also further confirmed by the IR spectra data (Fig. S5†). The single signal occurring at 2061 cm^{-1} in the FT-IR spectrum of **MOF-N_7**, which was not observed in the IR spectra of both NaN_3 or 4-FBN, was attributed to the anti-symmetric stretching vibration of the N_7^{3-} anion and such an assignment was in good agreement with the C_{2h} symmetry open-chain N_7^{3-} anion in **MOF-N_7**.

Crystal structure of α-Pb(N_3)$_2$. **α-Pb(N_3)$_2$** crystallizes in the orthorhombic space group *Pnma*, an asymmetric unit contains two independent Pb^{2+} atoms Pb1 and Pb2 (Pb2 located on the crystallographic mirror plane), four kinds of azide anions N_3^- (two of them are located on the crystallographic mirror plane) (Fig. S6†). Each Pb^{2+} ion is coordinated to eight N atoms from eight independent azide anions. Through the bridges comprised of the azide anions, the Pb^{2+} ions are linked together to form a 3D framework (Fig. 3).

Crystal structure of Pb-FBA. **Pb-FBA** crystallizes in the tetragonal space group $I4_1/a$. In the asymmetric unit of **Pb-FBA**, there are two independent Pb^{2+} ions, one O^{2-} ion and two FBA^- ligands (Fig. S7†). Each Pb^{2+} ion coordinates to five O atoms

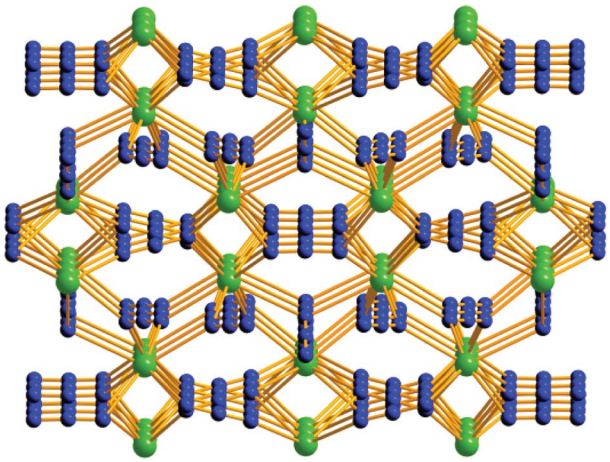

Fig. 3 A view of the 3D framework of α-$Pb(N_3)_2$.

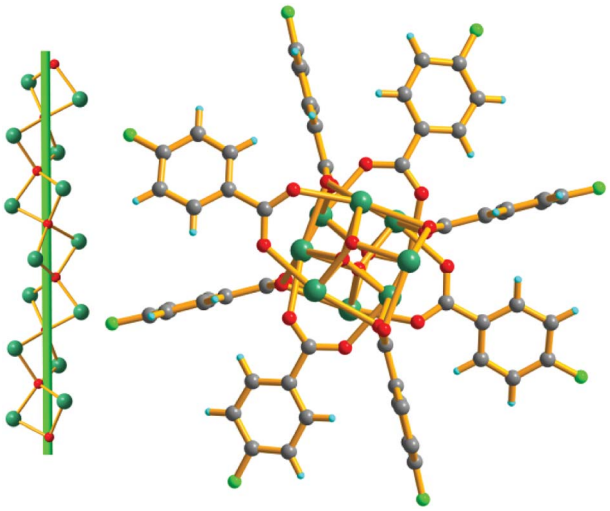

Fig. 4 A view of the 1D neutral 4_1-helical chain (right) constructed *via* the inorganic $[Pb_2O]^{2+}$ chain (left) and FBA^- ligands along the *c*-axis of **Pb-FBA**.

from two O^{2-} ions and three FBA^- ligands, respectively. The μ_4-O^{2-} anions link the adjacent Pb^{2+} ions to generate a $[Pb_2O]^{2+}$ cationic chain. The μ_2-FBA^- ligands encompass the cationic chain and lead to the formation of a neutral 4_1-helical chain *via* coordination to the Pb^{2+} ions running along the *c*-axis with a pitch of 10.773 Å (Fig. 4).

Mechanism of formation of the N_7^{3-} anion

As is well known, under hydrothermal conditions, the reaction of nitrile and azide using transition metal ions as a Lewis acid catalyst can lead to tetrazole ligands *via* an *in situ* [2 + 3] cycloaddition reaction mechanism,[28–33] in distinct contradiction with the *in situ* formed N_7^{3-} anion in **MOF-N_7**. The reaction mechanism of N_7^{3-} anion formation is proposed as follows (Scheme 1). The Lewis acid Pb^{2+} ion activates the azide *via* coordination to form an intermediate, which undergoes a reaction process, which is similar to the Ritter reaction[43,44] (a Ritter-like reaction) to generate an amide. Under the hydrothermal

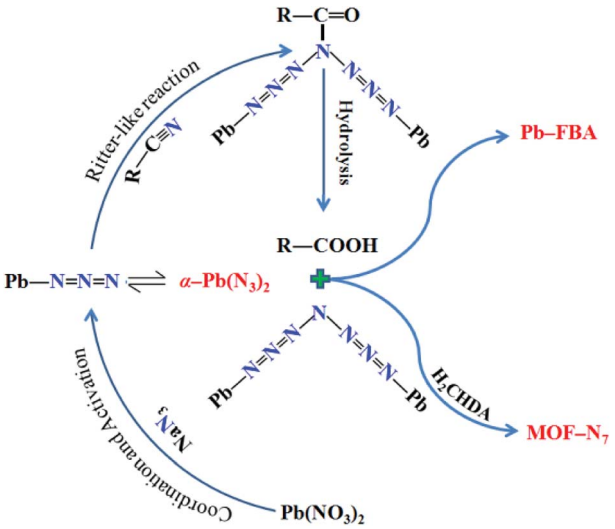

Scheme 1 The proposed mechanism of the formation of N_7^{3-} anion.

conditions, the amide was further hydrolyzed to give an amine and carboxylic acid, which were captured *via* coordination to the Pb^{2+} ions to form **MOF-N_7** and **Pb-FBA**, respectively. This is the first example of metal ions being used as a Lewis acid catalyst in the reaction between nitrile and azide for the *in situ* preparation of polynitrogens.

To verify the activation of azide by the Pb^{2+} ion, we considered two different activated models of Pb^{2+} with N_3^- and 4-FBN. The optimized stable structures were successfully obtained based on quantum chemical calculations. The optimized structures and interaction energies are summarized in Fig. S1 and Table S4,† respectively. The corrected interaction energies observed for **Pb⋯N_3** and **Pb⋯4-FBN** were found to be −316.48 and −106.18 kcal mol^{-1}, respectively, indicating that **Pb⋯N_3** was more favored in the reaction mixture of Pb^{2+}, N_3^- and 4-FBN. Furthermore, the calculated analysis was supported by the following experiments. Interestingly, a Pb^{2+} complex containing azide ions, **α-$Pb(N_3)_2$** was isolated. The preparation of **α-$Pb(N_3)_2$** was carried out using the procedure for preparing **MOF-N_7** with the addition of 4-FBN not included. Moreover, we also attempted to prepare the possible product containing Pb^{2+} and 4-FBN. Unfortunately, we failed to obtain the Pb^{2+} complex involving the 4-FBN ligand. It was noted that only a few complexes of Pb^{2+} and nitrile is available in the literature, which is probably due to the existence of only a weak coordination interaction between Pb^{2+} ion and the CN group. The above results suggest the possibility that the activation of azide by the Pb^{2+} ion occurred during the hydrothermal reaction process.

To further aid the understanding of the reaction mechanism of 4-FBN and NaN_3 with Pb^{2+} ion as a Lewis acid catalyst, electrostatic potential and electrostatic potential basins analyses were made for **Pb⋯N_3** and 4-FBN, which were based on theoretical calculations. As shown in Fig. 5, a positive potential occurs around the uncoordinated terminal N atom in **Pb⋯N_3** and a negative potential encompasses the N atom of the CN group in 4-FBN. The electrostatic potential values in the

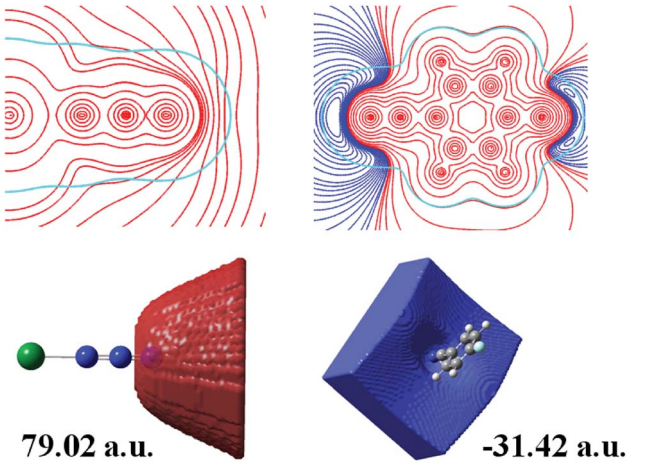

Fig. 5 A 2D representation of the molecular electrostatic potential (MEP) of Pb···N_3 and 4-FBN in the molecular plane (top) and electrostatic potential basins of the attractor and repulsor around the terminal N atom in Pb···N_3 and the N atom of the CN group in 4-FBN, respectively (bottom) (red, positive; blue, negative; cyan, 0.001 a.u. electron density isopotential line).

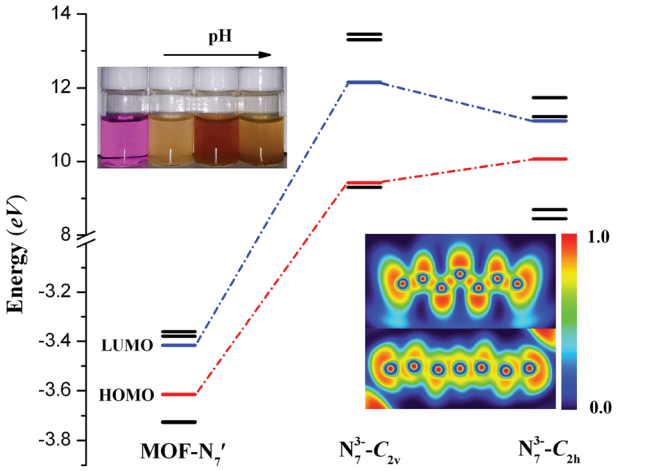

Fig. 6 The energy diagram for N_7^{3-}-C_{2h}, N_7^{3-}-C_{2v} and MOF-$N_{7'}$ (inset: the ELF contours illustrated on a plane of N_7^{3-}-C_{2v} (top), the N_7^{3-} anion fragment in MOF-N_7 (bottom) and the colorimetric changes in the $KMnO_4$ solution before and after the addition of MOF-N_7).

corresponding basins were 79.02 and −31.42 a.u., respectively. This suggests the possibility that the N atom of the CN group is an electron donor that interacts with the terminal N atom of **Pb···N_3**. The computational results also disclose that the activated **Pb···N_3** can attack the N atom of the CN group *via* the terminal N atom to form an amide by means of a Ritter-like reaction process (Scheme 1). Unfortunately, we have not directly isolated the amide product due to the amide produced being susceptible to hydrolysis under the hydrothermal reaction conditions to yield the amine and carboxylic acid. We only captured the amine and carboxylic acid yielded *via* coordination in **MOF-N_7** and **Pb-FBA**, respectively. **Pb-FBA** was obtained *via* the reaction of $Pb(NO_3)_2$ with 4-FBN and NaN_3 under the same reaction conditions used for the preparation of **MOF-N_7**. In addition, under the above reaction conditions, the prepared **α-Pb(N_3)$_2$** can also directly react with 4-FBN to form **Pb-FBA**. In the crystal of **Pb-FBA**, the *in situ* formed FBA^- ligand is the hydrolysis product of the amide intermediate produced. Based on the above three crystalline interrelated intermediates, **MOF-N_7**, **α-Pb(N_3)$_2$** and **Pb-FBA**, we further confirmed that the azide ion, rather than the nitrile was activated by the Pb^{2+} ion and this mechanism is a distinct contradiction with the previous results in which the nitrile reacts with azide in the presence of transition metal ions.[28–33]

Chemical and thermal stability of the N_7^{3-} anion

Furthermore, deeper insight into the nature of the N_7^{3-} anion and theoretical calculations were performed for **MOF-N_7**. In the DFT calculations, **MOF-$N_{7'}$** was taken from the crystal structure of **MOF-N_7**, where the symmetry of N_7^{3-} anion was C_{2h} and a minor calculation model was selected. The optimized stable structure of the N_7^{3-} anion was also obtained, which shows that the vibrationally stable N_7^{3-} anion possesses C_{2v} symmetry (**N_7^{3-}-C_{2v}**) and this calculated result was comparable to the theoretical analysis of N_7^- anion reported by others.[45,46] Fig. 6 exhibits the energies of the frontier molecular orbitals of three models, respectively. The energies of the HOMO of N_7^{3-} anion (**N_7^{3-}-C_{2h}**) in **MOF-N_7** and **N_7^{3-}-C_{2v}** are all larger, while that of **MOF-$N_{7'}$** is the smallest, indicating that both the formers can easily donate electrons. As expected, the free N_7^{3-} anion was unstable in the chemical process with electron transfer. For the latter, **MOF-$N_{7'}$** cannot readily donate electrons and possesses higher chemical stability, showing that N_7^{3-} anion can be captured *via* coordination. However, it can be easily oxidized by $KMnO_4$ solution (Fig. 6). Especially, it can react with basic $KMnO_4$ solution, meaning that **MOF-N_7** may be a good reducing agent in chemical reactions, which is also further evidence for the formation of N_7^{3-} anion stabilized in **MOF-N_7**.

Besides, the bonding patterns of N_7^{3-} anion and **MOF-$N_{7'}$** were explored *via* an intuitive map of the electron localization function (ELF). As shown in Fig. 6, for **N_7^{3}-C_{2v}**, the regions containing the maximum ELF values on the molecular plane can be identified as the lone pairs and six σ bonds. The π electrons located above and below the molecular plane are highly delocalized, which can also be directly observed *via* the EFL-π isosurface map (value = 0.70) contributed to from all the occupied π orbitals (Fig. S8†). When compared with **N_7^{3-}-C_{2v}**, the bonding features of the N_7^{3-} anion fragment in **MOF-$N_{7'}$** have distinct diversification. The regions with maximum ELF values for the lone pairs and six σ bonds are smaller, except for the lone pairs of the two terminal N atoms, indicating that the lone pairs and σ electrons as well as the π electrons were more highly delocalized and distributed around the whole N_7^{3-} anion chain (Fig. S8†). Clearly, the corresponding N–N bond distances in **N_7^{3-}-C_{2v}** (1.259, 1.278 and 1.407 Å) are also different from those of the N_7^{3-} anion fragment (1.198(31), 1.261(39) and 1.191(30) Å) in **MOF-N_7** (Fig. S2†). The experimental N–N bond lengths of the N_7^{3-} anion fragment, which are all within the range expected for predominantly covalent N–N bonds and indicate that the N_7^{3-} anion can be stabilized in the **MOF-N_7**.

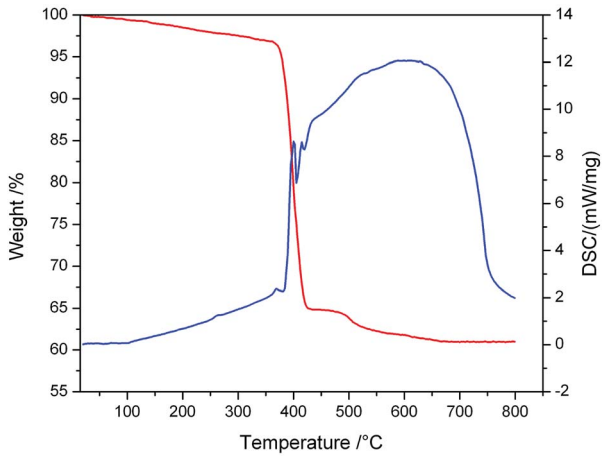

Fig. 7 The TGA/DSC plots obtained for **MOF-N_7** at a heating rate of 10 °C min^{-1} under a flow of N_2.

Additionally, the positive $\nabla^2\rho$ values, negative $H(r)$ values and $|V(r)|/G(r) > 1$ demonstrate that the Pb–N bonds have dominant covalent character whereas classical covalent character is observed for all the N–N bonds with negative $\nabla^2\rho$ and $H(r)$ values and $|V(r)|/G(r) > 2$ (Table S5†). Thus, the **MOF-N_7** and the N_7^{3-} anion have high thermal stability. The aforementioned results show that the formation of a metal complex can stabilize N_7^{3-} anion, which coincides with those ideas of other predicted metal complexes, such as $M^{4+}(\eta^6\text{-}N_6^{4-})$ (M = Ti, Zr, Hf, Th),[47] $Sc^{3+}(\eta^7\text{-}N_7^{3-})$[48] and $(\eta^5\text{-}N_5^{-})M^{4+}(\eta^7\text{-}N_7^{3-})$ (M = Ti, Zr, Hf, Th).[49] Therefore, the calculated dissociation energies of N_7^{3-} into N_2, for $\mathbf{N_7^{3-}}$-$\boldsymbol{C_{2h}}$ and $\mathbf{N_7^{3-}}$-$\boldsymbol{C_{2v}}$ are 645.08 and 440.13 kcal mol^{-1}, respectively, indicating that the N_7^{3-} anion lies much higher energetically than 7/2 N_2. All these findings coincide with the results obtained during TGA/DSC. The TGA shows that the framework of **MOF-N_7** was stable up to 369 °C and the N_7^{3-} anion starts to decompose up until 430 °C, accompanied by an exothermic enthalpy change of *ca.* 8.61 kJ g^{-1} (Fig. 7), which was more than two times greater than heats of detonation of TNT (3.75 kJ g^{-1}).[19,50] The high energy content of N_7^{3-} anion shows that **MOF-N_7** may be useful as an explosive just like other nitrogen-rich MOFs.

Conclusions

In summary, we have successfully prepared and captured a new N_7^{3-} anion for the first time, which has been studied using FT-IR, single-crystal XRD and theoretical calculations. The N_7^{3-} anion in **MOF-N_7** possesses excellent thermal stability and the high energy N_7^{3-} anion was stabilized by coordination interactions with Pb^{2+} ions. Our study is the first to reveal that transition metal ions and main group Pb^{2+} ions show different activation mechanisms in the *in situ* reaction of metal ions with azide and nitrile, and this distinction was due to the different interactions between the metal ion and azide/nitrile. The weak interaction between transition metal ions and azide results in the metal ion activating the nitrile, and thus, giving the tetrazole product. Whereas the strong interactions between Pb^{2+} ion and azide gives rise to the azide ion being activated *via* a coordination interaction with the Pb^{2+} ion, accordingly, producing polynitrogen anions. The successful synthesis and coordination capture of N_7^{3-} anion as well as the reaction mechanism study will not only be an important milestone towards one ultimate goal of preparing new polynitrogens, but also provides promising insights into the mechanism of metal catalysis in the *in situ* formation of polynitrogens. In addition, this work brings fresh design ideas to polynitrogen molecules and nitrogen-rich MOFs as energetic materials of the future.

Conflicts of interest

The authors declare no competing financial interest.

Acknowledgements

We thank the Natural Science Foundation of the Education Commission of Anhui Province of China (No. KJ2017A347) and the Program for Innovative Research Team in Anqing Normal University for financial support.

Notes and references

1 J. R. Li, R. J. Kuppler and H. C. Zhou, *Chem. Soc. Rev.*, 2009, **38**, 1477–1504.
2 J. R. Li, J. Sculley and H. C. Zhou, *Chem. Rev.*, 2012, **112**, 869–932.
3 R. B. Getman, Y. S. Bae, C. E. Wilmer and R. Q. Snurr, *Chem. Rev.*, 2012, **112**, 703–723.
4 M. P. Suh, H. J. Park, T. K. Prasad and D.-W. Lim, *Chem. Rev.*, 2012, **112**, 782–835.
5 J. Lee, O. K. Farha, J. Roberts, K. A. Scheidt, S. T. Nguyen and J. T. Hupp, *Chem. Soc. Rev.*, 2009, **38**, 1450–1459.
6 M. Yoon, R. Srirambalaji and K. Kim, *Chem. Rev.*, 2012, **112**, 1196–1231.
7 L. E. Kreno, K. Leong, O. K. Farha, M. Allendorf, R. P. Van Duyne and J. T. Hupp, *Chem. Rev.*, 2012, **112**, 1105–1125.
8 D. Liu, K. Lu, C. Poon and W. Lin, *Inorg. Chem.*, 2014, **53**, 1916–1924.
9 W. J. Shi, L. Y. Du, H. Y. Yang, K. Zhang, L. Hou and Y. Y. Wang, *Inorg. Chem.*, 2017, **56**, 10090–10098.
10 M. H. Teplensky, M. Fantham, P. Li, T. C. Wang, J. P. Mehta, L. J. Young, P. Z. Moghadam, J. T. Hupp, O. K. Farha, C. F. Kaminski and D. Fairen-Jimenez, *J. Am. Chem. Soc.*, 2017, **139**, 7522–7532.
11 A. Phan, C. J. Doonan, F. J. Uribe-Romo, C. B. Knobler, M. O'Keeffe and O. M. Yaghi, *Acc. Chem. Res.*, 2010, **43**, 58–67.
12 Z. Zheng, X. Jiang and J. Zhao, *Chem. Phys. Lett.*, 2015, **628**, 76–80.
13 L. H. Blair, A. Colakel, R. M. Vrcelj, I. Sinclair and S. J. Coles, *Chem. Commun.*, 2015, **51**, 12185–12188.
14 X. Qu, S. Zhang, Q. Yang, Z. Su, Q. Wei, G. Xie and S. Chen, *New J. Chem.*, 2015, **39**, 7849–7857.
15 S. Zhang, X. Liu, Q. Yang, Z. Su, W. Gao, Q. Wei, G. Xie, S. Chen and S. Gao, *Chem.–Eur. J.*, 2014, **20**, 7906–7910.

16 O. S. Bushuyev, G. R. Peterson, P. Brown, A. Maiti, R. H. Gee, B. L. Weeks and L. J. Hope-Weeks, *Chem.–Eur. J.*, 2013, **19**, 1706–1711.
17 Z. Liu, T. Zhang, J. Zhang and S. J. Wang, *J. Hazard. Mater.*, 2008, **154**, 832–838.
18 S. Li, Y. Wang, C. Qi, X. Zhao, J. Zhang, S. Zhang and S. Pang, *Angew. Chem., Int. Ed.*, 2013, **52**, 14031–14035.
19 W. Gao, X. Liu, Z. Su, S. Zhang, Q. Yang, Q. Wei, S. Chen, G. Xie, X. Yang and S. Gao, *J. Mater. Chem.*, 2014, **2**, 11958–11965.
20 S. Chen, S. Shu and S. Gao, *Inorg. Chim. Acta*, 2009, **362**, 3043–3408.
21 K. L. Zhang, Z. C. Pan, Y. Chang, W. L. Liu and S. W. Ng, *Mater. Lett.*, 2009, **63**, 2136–2138.
22 J. D. Lin, S. H. Wang, L. Z. Cai, F. K. Zheng, G. C. Guo and J.-S. Huang, *CrystEngComm*, 2013, **15**, 903–910.
23 Y. Feng, X. Liu, L. Duan, Q. Yang, Q. Wei, G. Xie, S. Chen, X. Yang and S. Gao, *Dalton Trans.*, 2015, **44**, 2333–2339.
24 J. Zhang, H. Su, Y. Dong, P. Zhang, Y. Du, S. Li and S. Pang, *Inorg. Chem.*, 2017, **56**, 10281–10289.
25 L. Batzdorf, F. Fischer, M. Wilke, K. J. Wenzel and F. Emmerling, *Angew. Chem., Int. Ed.*, 2015, **54**, 1799–1802.
26 R. Uematsu, E. Yamamoto, S. Maeda, H. Ito and T. Taketsugu, *J. Am. Chem. Soc.*, 2015, **137**, 4090–4099.
27 P. Verma, K. D. Vogiatzis, N. Planas, J. Borycz, D. J. Xiao, J. R. Long, L. Gagliardi and D. G. Truhlar, *J. Am. Chem. Soc.*, 2015, **137**, 5770–5781.
28 D. C. Zhong, Y. Q. Wen, J. H. Deng, X. Z. Luo, Y. N. Gong and T. B. Lu, *Angew. Chem., Int. Ed.*, 2015, **54**, 11795–11799.
29 Z. P. Demko and K. B. Sharpless, *Angew. Chem., Int. Ed.*, 2002, **41**, 2110–2113.
30 Z. P. Demko and K. B. Sharpless, *Angew. Chem., Int. Ed.*, 2002, **41**, 2113–2116.
31 R. G. Xiong, X. Xue, H. Zhao, X. Z. You, B. F. Abrahams and Z. Xue, *Angew. Chem., Int. Ed.*, 2002, **41**, 3800–3803.
32 H. Zhao, Z. R. Qu, H. Y. Ye and R. G. Xiong, *Chem. Soc. Rev.*, 2008, **37**, 84–100.
33 F. Himo, Z. P. Demko, L. Noodleman and K. B. Sharpless, *J. Am. Chem. Soc.*, 2003, **125**, 9983–9987.
34 G. M. Sheldrick, SHELXL-2014/7, Program for the refinement of crystal structures, *Acta Crystallogr.*, 2015, **71**, 9–18.
35 M. J. Frisch, G. W. Trucks, H. B. Schlegel, G. E. Scuseria, M. A. Robb, J. R. Cheeseman, G. Scalmani, V. Barone, B. Mennucci, G. A. Petersson, H. Nakatsuji, M. Caricato, X. Li, H. P. Hratchian, A. F. Izmaylov, J. Bloino, G. Zheng, J. L. Sonnenberg, M. Hada, M. Ehara, K. Toyota, R. Fukuda, J. Hasegawa, M. Ishida, T. Nakajima, Y. Honda, O. Kitao, H. Nakai, T. Vreven, J. A. Montgomery Jr., J. E. Peralta, F. Ogliaro, M. Bearpark, J. J. Heyd, E. Brothers, K. N. Kudin, V. N. Staroverov, R. Kobayashi, J. Normand, K. Raghavachari, A. Rendell, J. C. Burant, S. S. Iyengar, J. Tomasi, M. Cossi, N. Rega, J. M. Millam, M. Klene, J. E. Knox, J. B. Cross, V. Bakken, C. Adamo, J. Jaramillo, R. Gomperts, R. E. Stratmann, O. Yazyev, A. J. Austin, R. Cammi, C. Pomelli, J. W. Ochterski, R. L. Martin, K. Morokuma, V. G. Zakrzewski, G. A. Voth, P. Salvador, J. J. Dannenberg, S. Dapprich, A. D. Daniels, O. Farkas, J. B. Foresman, J. V. Ortiz, J. Cioslowski and D. J. Fox, *Gaussian 09, Revision D.01*, Gaussian, Inc., Wallingford, CT, 2013.
36 A. D. Becke, *Phys. Rev. A*, 1998, **38**, 3098–3100.
37 C. Lee, W. Yang and R. G. Parr, *Phys. Rev. B*, 1988, **37**, 785–789.
38 D. Andrae, U. Häußerman, M. Dolg, H. Stoll and H. Preuß, *Theor. Chim. Acta*, 1990, **77**, 123–141.
39 A. V. Marenich, C. J. Cramer and D. G. Truhlar, *J. Phys. Chem. B*, 2009, **113**, 6378–6396.
40 S. F. Boys and F. Bernardi, *Mol. Phys.*, 1970, **19**, 553–566.
41 T. Lu and F. W. Chen, *J. Comput. Chem.*, 2012, **33**, 580–592.
42 R. F. W. Bader *Atoms in molecules, a quantum theory*, Oxford University Press, Oxford, 1990.
43 J. J. Ritter and P. P. Minieri, *J. Am. Chem. Soc.*, 1948, **70**, 4045–4048.
44 J. J. Ritter and J. Kalish, *J. Am. Chem. Soc.*, 1948, **70**, 4048–4050.
45 H. H. Michels, J. A. Montgomery, K. O. Christe and D. A. Dixon, *J. Phys. Chem.*, 1995, **99**, 187–194.
46 Y. D. Liu, J. F. Zhao and Q. S. Li, *Theor. Chem. Acc.*, 2002, **107**, 140–146.
47 M. Straka, *Chem. Phys. Lett.*, 2002, **358**, 531–536.
48 L. Gagliardi and P. Pyykkö, *J. Am. Chem. Soc.*, 2001, **123**, 9700–9701.
49 L. Gagliardi and P. Pyykkö, *J. Phys. Chem. A*, 2002, **106**, 4690–4694.
50 O. S. Bushuyev, P. Brown, A. Maiti, R. H. Gee, G. R. Peterson, B. L. Weeks and L. J. Hope-Weeks, *J. Am. Chem. Soc.*, 2012, **134**, 1422–1425.

